Nuclear Instruments and Methods in Physics Research B 580 (2026) 166252

Contents lists available at ScienceDirect

Nuclear Inst. and Methods in Physics Research, B

journal homepage: www.elsevier.com/locate/nimb

Full length article

Validation of proton energy loss in regolith simulants: PSI Proton Irradiation Facility (PIF) beam tests and MRADSIM simulations

Zehra Guzel [a,c], Muhammad Waqas [c], Ali Behcet Alpat [b,c,*], Talifujiang Wusimanjiang [c], Celal Mert Okan [c], Deniz Dolek [c], Efe Alpat [c], Mariano Casu [d], Roberto Orrù [d], Giacomo Cao [d], Wojtek Hajdas [e,f], Radoslaw Marcinkowski [e]

[a] *Energy Institute, Istanbul Technical University, Sariyer, Istanbul, Turkey*
[b] *Istituto Nazionale di Fisica Nucleare (INFN), Perugia, Italy*
[c] *Beamide S.r.l., Via Campo di Marte 4/O, 06124, Perugia, Italy*
[d] *Dipartimento di Ingegneria Meccanica, Chimica e dei Materiali, Università degli Studi di Cagliari, Via Marengo 2, 09123, Cagliari, Italy*
[e] *SE2S, Fahrstrasse 9, 5314, Kleindöttingen, Switzerland*
[f] *Paul Sherrer Institute, Forschungsstrasse 11, 5232, Villigen, Switzerland*

ARTICLE INFO

Keywords:
Regolith simulants
Martian radiation
Martian habitat
In-situ resource utilization

ABSTRACT

This technical report documents the comparison and validation of proton-beam measurements performed at the Paul Sherrer Institute (PSI) Proton Irradiation Facility (PIF) with MRADSIM simulations for Martian regolith simulants once processed by Spark Plasma Sintering at the University of Cagliari. Thin targets of two regolith formulations (MGS-1 and JEZ-1) with thicknesses of 2 mm and 3 mm were irradiated under multiple degrader settings, spanning approximately 30–151 MeV proton energies at the regolith surface. Experimental detector-response spectra were calibrated using regolith-free reference runs, and peak energies were extracted using Gaussian fits. The PIF geometry was imported into MRADSIM toolkit via GDML, and the regolith simulants were implemented as composite materials. Simulated detector observables were obtained in a downstream 50 mm-thick LYSO scintillator detector volume, enabling direct experiment–simulation benchmarking of the peak deposited energy and the transmitted-proton fluence. In addition, several Geant4 hadronic physics lists were evaluated using a reduced chi-square (χ^2/ν) analysis to select a robust baseline model for regolith transport within the validated energy range.

1. Introduction

Human activities on Mars will take place in a radiation environment that is fundamentally different from Earth's, with limited atmospheric shielding and continuous exposure to energetic charged particle [1,2]. Among these, protons represent a major contribution over a wide energy range and are a primary driver of dose, material degradation, and secondary-particle production in surface and near-surface scenarios [3]. Given the availability of regolith in situ and its potential use as both a structural and shielding materials [2,4], a quantitative description of proton transport through realistic regolith simulants is required for credible shielding design and radiation risk assessment [5].

Accurate Monte Carlo modeling of proton transport through Martian regolith simulants is required to establish validated simulation settings for subsequent radiation-transport studies [6,7]. Proton-beam measurements performed at the Proton Irradiation Facility provide such a benchmark for thin-target energy degradation and transmission [8]. In these experiments, regolith simulant samples were irradiated under multiple degrader configurations, producing a set of well-defined incident conditions spanning approximately 50–151 MeV at the regolith surface. Two regolith simulants were studied—MGS-1 and JEZ-1—after being processed via Spark Plasma Sintering (SPS) to obtain dense samples, according to Casu et al. [9]. In particular this study focuses on thin regolith targets (2–3 mm thick) and assesses agreement between calibrated experimental energies and simulated detector observables, including energy deposition and proton fluence.

Monte Carlo simulation was performed taking advantage of MRADSIM [10], a Geant4-based [11] framework designed for radiation transport and shielding analyses. This software provides tools to work with complex 3D geometries (including GDML-based models), define materials and radiation sources, and extract detector-level quantities through scoring. Depending on the module and configuration, this software supports the evaluation of key observables such as deposited energy

* Corresponding author at: Istituto Nazionale di Fisica Nucleare (INFN), Perugia, Italy.
E-mail address: alpat@infn.it (A.B. Alpat).

https://doi.org/10.1016/j.nimb.2026.166252
Received 17 March 2026; Received in revised form 2 July 2026; Accepted 14 July 2026

and particle fluence (and, more generally, dose-related quantities), with options for component-based and 3D-mapped analyses [12,13]. In Section 2.4, the simulation setup adopted for the PIF benchmark (geometry import, material definitions, source, and scoring) is presented. The goal of this report is to reproduce and validate these measurements using MRADSIM simulations, providing a controlled experiment–simulation comparison before applying the same modeling chain to more complex Martian radiation scenarios. The experimental geometry supplied by PIF was imported in GDML form to preserve the beamline layout and material arrangement. The regolith simulants were implemented as composite materials in simulation framework according to oxide weight fractions indicated by the producer [14,15] and the densities of the produced SPS samples. Downstream scoring was performed in a 50 mm thick LYSO detector volume, providing a consistent definition of transmitted-proton energy deposition and fluence across all configurations. This setup enables direct, like-for-like comparison of (i) deposited energy and (ii) transmitted-proton fluence between experiment and simulation across regolith types, thicknesses, and incident energies.

Beyond agreement at the observable level, a second objective is to identify a robust hadronic physics [16] configuration for proton transport in this validated energy regime. Because simulation is based on Geant4(version 11.3.0) [17], physics-list selection can lead to measurable differences in predicted energy deposition and transmission, which is critical when quantifying regolith shielding effectiveness. For this reason, several candidate hadronic physics lists were benchmarked against the PIF dataset and ranked using a quantitative goodness-of-fit criterion (reduced chi-square with combined experimental and simulation uncertainties). The outcome of this benchmarking step is used to justify the baseline physics list adopted for subsequent regolith-transport analyses within the same validated energy range.

The scope of this work is the modeling validation performed against PIF thin regolith targets (2–3 mm thick) using proton energy deposition and fluence observables. This provides a controlled test of proton transport and detector response over the energy range considered. Extensions to broader Martian environmental spectra (including secondary neutrons and wider particle mixtures) should be treated as a subsequent step built on the validated foundation established in this report.

The remainder of the paper is organized as follows. Section 2 describes the PIF experimental configuration, the regolith sample preparation and material definitions, the detector-response calibration procedure, the MRADSIM implementation of the experimental setup, and the physics-list benchmarking methodology. Section 3 presents the experimental detector-response results, the simulated energy-deposition and transmitted-proton fluence spectra, the Geant4 physics-list comparison used to select the baseline model, and the quantitative experimental–simulation comparison across the tested degrader and regolith configurations. Finally, Section 4 summarizes the main validation outcomes and discusses the relevance of the validated modeling chain for subsequent Martian regolith radiation-transport studies.

2. Materials and methods

2.1. Experimental configuration at PIF

The experimental data analyzed in this study are originated from proton irradiation experiments conducted at PIF [8]. The experimental campaign, including beam delivery, detector operation, and data acquisition, was performed by the SE2S team. A proton beam with a primary energy of 200 MeV upstream of the degrader was delivered to the experimental line and propagated from left to right (see schematic in Fig. 1). The incident beam energy at the regolith sample was tuned by selecting dedicated copper (Cu) degrader configurations with different total thicknesses; each degrader setting produced a distinct energy spectrum at the regolith surface. The transmitted energy spectrum was measured with a ΔE–E (dE–E) nuclear telescope placed directly

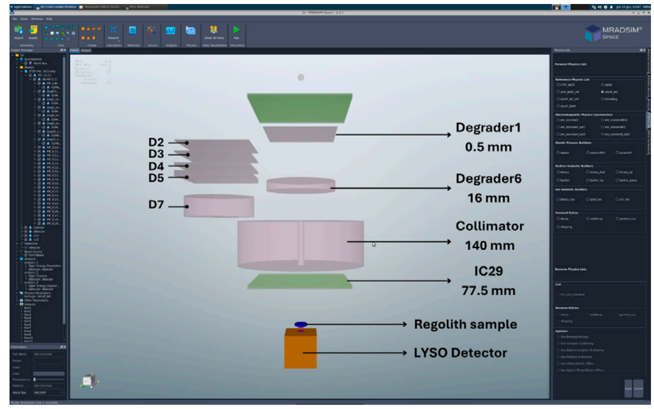

Fig. 1. Schematic view of the PIF proton irradiation setup. The beam passes through an ionization chamber, a set of degraders (Degrader1, D2, D3, D4, D5, Degrader6, D7), and a collimator before irradiating the regolith target and the downstream detector.

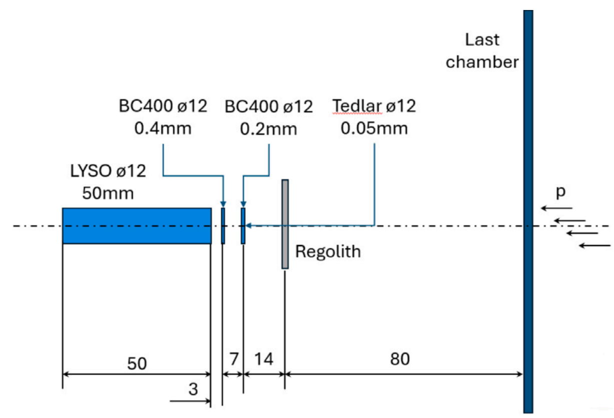

Fig. 2. PIF experimental detection setup. Protons propagate from right to left and traverse the regolith before entering the downstream telescope comprising BC400 scintillators and a Tedlar layer, with the signal recorded in a ∅12 mm, 50 mm-thick LYSO detector.

behind the sample. The Fig. 2 illustrates the experimental geometry and detection system; the reported data correspond to the 50 mm-thick LYSO detector [18]. Representative photographs of the actual experimental arrangement are shown in Fig. 3, where the regolith sample is positioned immediately upstream of the LYSO detector and aligned with the ionization chamber along the beam axis.

2.2. Regolith samples and thickness configurations

The PIF datasets correspond to proton irradiation measurements of two Martian regolith simulant compositions. To obtain the 2 and 3 mm thick dense samples, original powders were sintered via SPS at 1050 °C –35 MPa and 1100 °C –15 MPa for the cases of MGS-1 and JEZ-1, respectively [9]. Oxide composition and final achieved densities (2.74 g/cm^3 for MGS-1 and 2.80 g/cm^3 for JEZ-1) are given in Table 1. Multiple degrader configurations (given in Table 3) were used to modify the incident proton energy prior to its interaction with the target. Regolith-free reference measurements were provided for identical degrader settings and were used as the baseline for the detector energy calibration. The dataset corresponding to measurements performed without regolith comprises 12 copper degrader configurations with total thicknesses ranging from 16.5 to 42.0 mm (16.5, 19.5, 20.5, 25.0, 28.0, 30.0, 32.5, 34.5, 36.5, 39.5, 40.5, and 42.0 mm). Experiments including regolith were conducted only for total thicknesses of 16.5, 28.0, 36.5, and 39.5 mm (see Table 3).

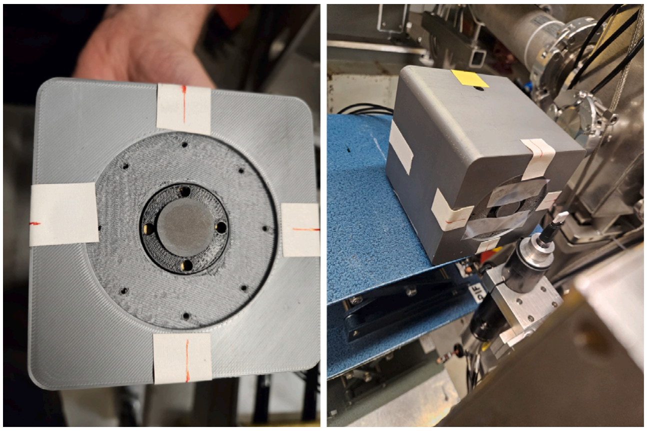

Fig. 3. On the left, the regolith sample is mounted immediately upstream of the LYSO detector. On the right, an ionization chamber, the regolith sample, and the LYSO detector are mounted along the beam axis.

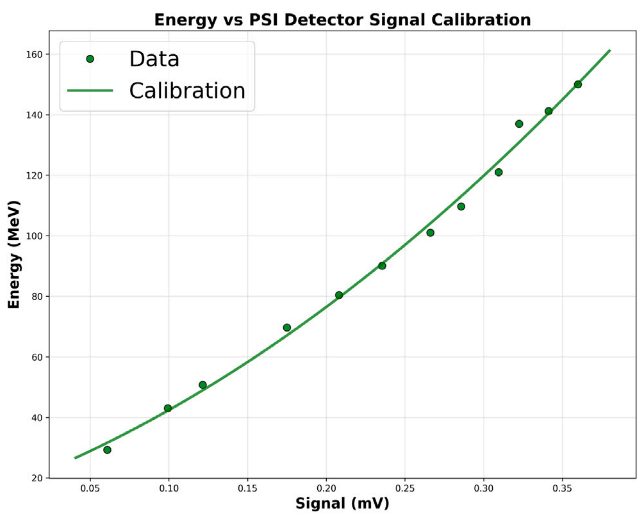

Fig. 4. Energy calibration obtained from regolith-free reference measurements, showing the quadratic relationship between detector response amplitude (U_{MPV}) and proton energy. The fitted calibration function was applied to all experimental datasets.

2.3. *Data acquisition and energy calibration*

Experimental data were provided in the form of detector signal amplitude spectra expressed in millivolts (mV). The detector response was converted to proton energy using a calibration derived from regolith-free reference measurements. The main peak in each spectrum was fitted with a Gaussian function to extract the peak position U_{MPV} and width. The fitted calibration function was applied consistently to all experimental spectra across degrader configurations, regolith types, and thicknesses (see Fig. 4). Regolith-free reference data were additionally used to establish the relationship between degrader thickness and proton energy (see Fig. 5), which defines the proton energy at the regolith surface $E_{surface}$ for each configuration.

2.4. *MRADSIM simulation framework*

MRADSIM (Matter-RADiation Interactions SIMulations) is a modular simulation software toolkit developed to numerically evaluate radiation effects in electronic components, human tissues, and a wide range of materials. Its goal is to model radiation–matter interactions

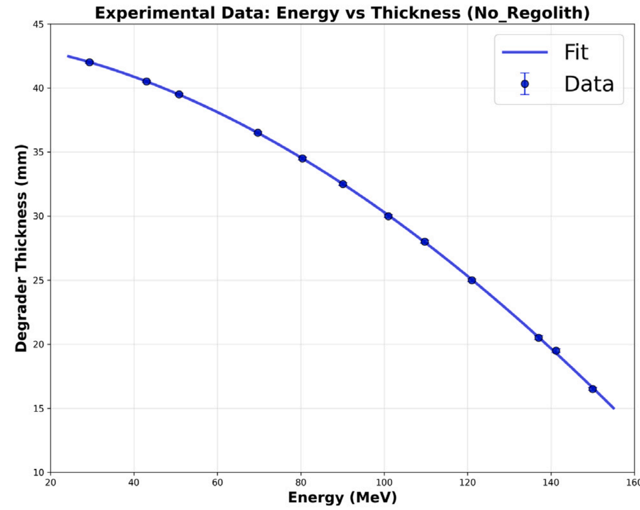

Fig. 5. Relationship between degrader thickness and proton energy derived from regolith-free measurements, used to define the surface energy ($E_{surface}$) for each degrader configuration.

with high parameter control, reduce computational cost, and provide application-specific analysis capabilities, especially for space missions. The MRADSIM ecosystem includes a geometry converter that translates CAD models (e.g., STEP) into GDML for simulation, as well as dedicated packages such as MRADSIM-Dose for dose/energy-deposition outputs and MRADSIM-Space for space-radiation applications. In MRADSIM-Space, Geant4-based particle transport is performed within the defined geometry to compute metrics such as dose, fluence, LET spectra/flux, charging, and 3D depth-dose distributions [10]. In this work MRADSIM is used to reproduce the experimental proton irradiation setup and to model proton interactions with regolith simulant materials. The experimental geometry provided by PIF in GDML format was imported into simulation framework as the baseline setup. While the beamline layout and overall geometry were preserved, the regolith sample materials were redefined to implement composite material models for MGS-1 and JEZ-1 (for details, see Section 2.5). The primary source was defined in simulation framework as a monoenergetic proton point beam with an initial energy of 200 MeV. The beam was emitted from $(x, y, z) = (0, 0, 365)\,\mathrm{mm}$ and directed along the $-Z$ axis with $\theta = 0°$. For each configuration, 10^6 primary protons were simulated, with no additional source normalization applied. Separate simulation configurations were generated for each copper degrader setting and regolith thickness. After the physics list benchmarking described in Section 2.6, `QGSP_BIC` was adopted as the baseline physics list for the final proton transport simulations.

Detector definition. To represent the experimental telescope detector, a downstream LYSO detector volume was modeled as the scoring region. The scintillator layers were modeled as cylindrical volumes with dimensions ($r = 6\,\mathrm{mm}$, $t = 0.2\,\mathrm{mm}$) and ($r = 6\,\mathrm{mm}$, $t = 0.4\,\mathrm{mm}$), respectively, using the `Plastic_SC_Vinyltoluene` material, while the LYSO detector was modeled as a $(50 \times 50 \times 50)\,\mathrm{mm}^3$ box made of `Lutetium_Yttrium_OxyorthoSilicate` (LYSO). Simulated observables include (i) the energy-deposition spectrum in the LYSO volume and (ii) the transmitted-proton fluence spectrum, extracted using an identical scoring definition for all configurations. As shown in Fig. 6, the simulation represents the experimental geometry and detector system.

2.5. *Regolith material modeling*

MGS-1 and JEZ-1 regolith simulants were implemented as composite materials in simulation framework. Individual oxide constituents

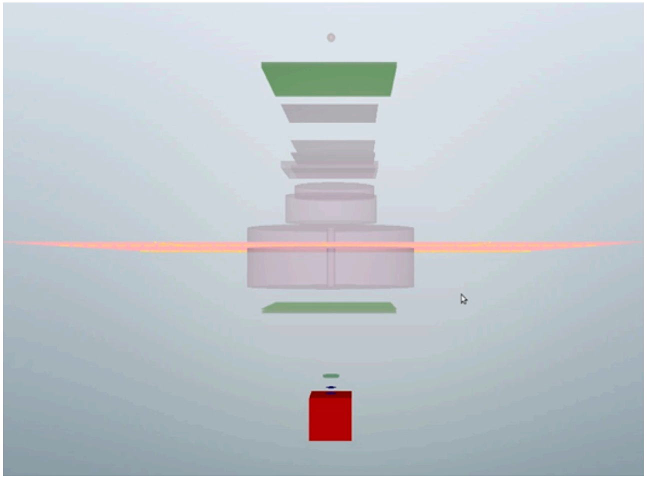

Fig. 6. Simulation software visualization of the imported PIF geometry and scoring setup. Simulated observables were collected in the downstream 50 mm thick LYSO detector volume.

Table 1
Regolith simulant compositions (wt.%) and bulk density of MGS-1 and JEZ-1 Martian regolith simulants used in Simulation framework.

Compound	MGS-1	JEZ-1
SiO_2	45.57	44.2
Al_2O_3	9.43	11.3
FeO	16.85	9.5
MnO	0.10	0.10
MgO	16.5	25.9
CaO	4.03	3.5
Na_2O	3.66	1.9
K_2O	0.43	0.3
TiO_2	0.30	0.2
P_2O_5	0.37	0.6
Cr_2O_3	0.12	0.3
SO_3	2.63	2.1
Sintered sample density (g/cm^3)	2.74	2.80

were defined using NIST-based material definitions and combined according to their weight fractions, as reported by the producers [14,15]. Samples densities were estimated with the Archimedes' method. Table 1 summarizes the material definitions used in this report.

2.6. Benchmarking of simulation data against Geant4 physics models

This analysis aimed to identify the most robust GEANT4 physics list for simulating the interaction of the broader Martian radiation environment with regolith shielding. Several candidate Geant4 hadronic physics lists (FTFP_BERT, QGSP_BERT, QGSP_BERT_HP, QGSP_BIC, QGSP_BIC_HP, Shielding, QBBC) were benchmarked against the PIF experimental dataset for JEZ-1 targets at 2 mm and 3 mm thickness [16]. Table 2 summarizes the energy-deposition results (MeV) in the LYSO detector for JEZ-1 at regolith thicknesses of 2 mm and 3 mm across all tested physics lists. These results are presented in Section 3.3.

The mathematical framework employed for benchmarking the physics lists against experimental proton beam data, based on a reduced chi-square (χ^2/ν) analysis, is implemented through a weighted least-squares linear regression. For each physics list and thickness, simulated energy deposition values y_i (with uncertainty $\sigma_{y,i}$) measured in the LYSO detector were compared to experimental calibration energies x_i (with uncertainty $\sigma_{x,i}$) using a weighted linear model,

$$y = mx_i + c \tag{1}$$

where m is the slope, c is the intercept. The total uncertainty for each measurement is calculated by combining experimental and simulation uncertainties in quadrature,

$$\sigma_{\text{tot},i} = \sqrt{\sigma_{x,i}^2 + \sigma_{y,i}^2}\,. \tag{2}$$

Weighted linear regression was performed to determine the optimal parameters m and c by minimizing the chi-square statistic,

$$\chi^2 = \sum_{i=1}^{n} \frac{\left(y_i - (mx_i + c)\right)^2}{\sigma_{\text{tot},i}^2} \tag{3}$$

where n is the number of data points (4 points per thickness). The reduced chi-square is then computed as,

$$\chi_\nu^2 = \chi^2/\nu \tag{4}$$

where the degrees of freedom $\nu = n - 2$ (two parameters estimated: m and c). Based on this analysis, the `QGSP_BIC` model is recommended as the optimal overall physics list for Martian radiation simulations. The combined χ^2 values for the 2 mm and 3 mm configurations indicate that `QGSP_BIC` demonstrates the most balanced performance across different regolith thicknesses [19]. Consequently, `QGSP_BIC` is selected as the primary validated physics model for all subsequent PIF benchmark analyses. The complete set of benchmarking results is presented in Section 3.3.

3. Results

3.1. Experimental results

This section presents the experimental results from the PIF proton beam measurements, including the detector response spectra and the derived energy-deposition trends for MGS-1 and JEZ-1 regolith samples. Fig. 7 presents representative experimental detector response spectra provided by PIF for a nominal proton energy of 50.8 MeV, corresponding to MGS-1 regolith thicknesses of 2 mm and 3 mm, as well as a reference measurement without regolith. Gaussian fits were applied to the main spectral peaks to extract peak positions and widths. An increasing regolith thickness results in a systematic shift of the peak toward lower detector response values, reflecting enhanced energy loss in the material. The spectra shown are representative examples, and the same analysis procedure was consistently applied to all experimental datasets for different degrader configurations, regolith types (MGS-1 and JEZ-1), and material thicknesses.

Fig. 8 shows the relationship between the measured proton energy at the regolith surface (E_{surface}) and the deposited energy of detector (E_{det}) for MGS-1 and JEZ-1 regolith samples with thicknesses of 2 mm and 3 mm. The detector energies were determined using the no-regolith calibration described in 2.3. The dashed red line represents the case $E_{\text{det}} = E_{\text{surface}}$, corresponding to the absence of energy loss in the regolith. For both regolith types, the measured energies lie systematically below the $y = x$ reference line, indicating energy loss within the material. A larger deviation is observed for the 3 mm samples compared to the 2 mm samples, demonstrating the thickness-dependent energy degradation, as expected for these materials [5]. As the proton energy increases, the difference between E_{det} and E_{surface} decreases, demonstrating that the regolith becomes increasingly transparent to higher energy protons and its energy degrading effect diminishes. A systematic difference between JEZ-1 and MGS-1 regolith samples is observed, reflecting differences in material composition and effective density. These differences lead to slightly different energy loss behaviors for the same regolith thickness, highlighting the sensitivity of the measurements to regolith material properties.

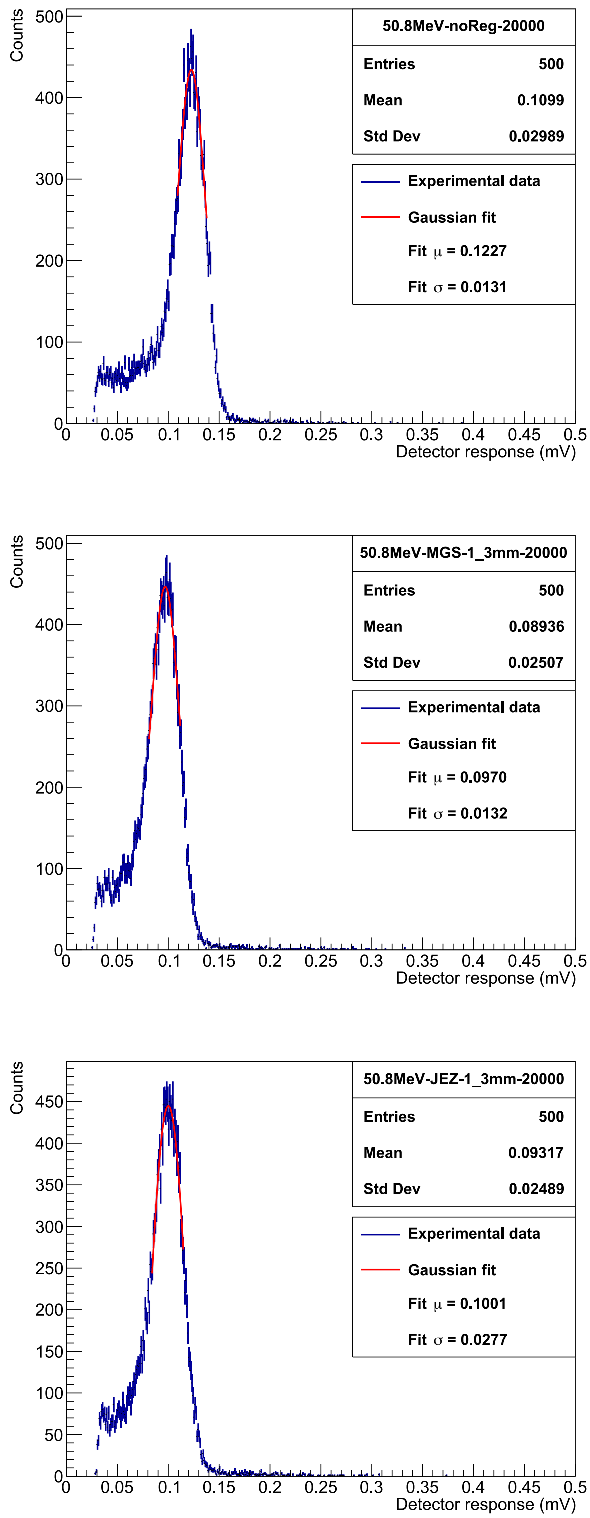

Fig. 7. Representative experimental detector response spectra provided by PIF for a nominal proton energy of 50.8 MeV. The spectra include a reference measurement without regolith and measurements performed with JEZ-1 and MGS-1 regolith samples of 2 mm and 3 mm thickness. The detector response is shown as a function of signal amplitude, and Gaussian fits are applied to the main peaks for the extraction of peak position and width parameters.

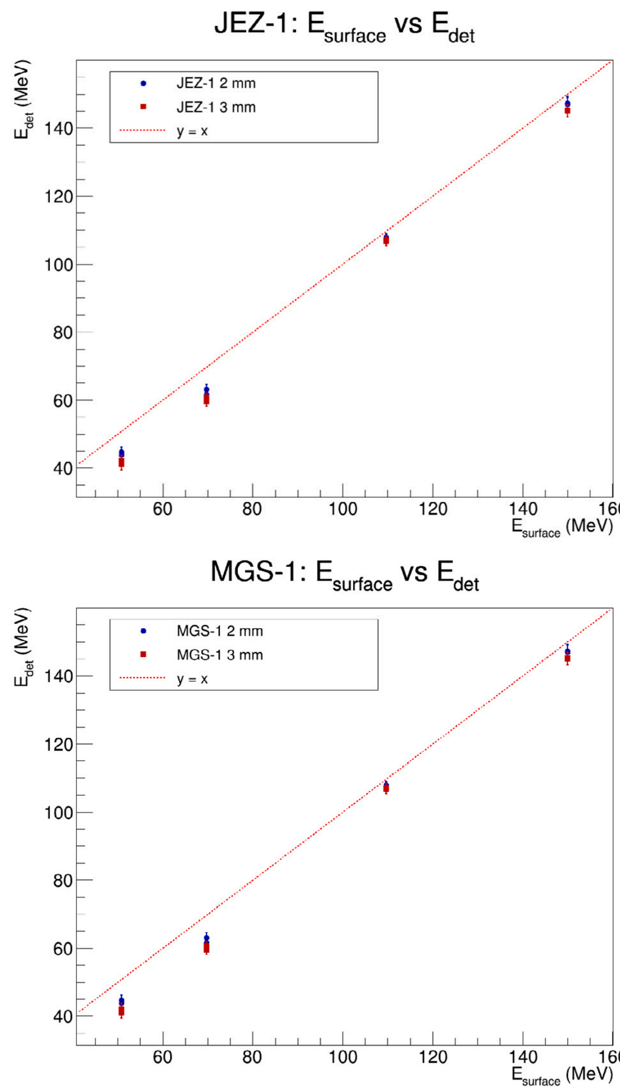

Fig. 8. Deposited energy of detector (E_{det}) as a function of proton energy at the regolith surface ($E_{surface}$) for (a) MGS-1 and (b) JEZ-1 regolith samples with thicknesses of 2 mm and 3 mm.

3.2. Simulation results

A consistent analysis of energy deposition and transmitted-proton fluence was adopted to derive comparable detector observables from the simulations for validation against the experimental calibration data. Simulated energy deposition and transmitted-proton fluence spectra were extracted in the LYSO detector volume using identical scoring definitions across configurations. The spectra shown in Figs. 9 and 10 are representative examples selected to demonstrate the scoring and peak-extraction procedure; the same Gaussian-fitting workflow was applied consistently to all simulated configurations (degrader settings, regolith types, and thicknesses).

Fig. 9 shows the simulated energy-deposition spectra in the LYSO detector for the 36.5 mm degrader configuration, for (a) no regolith, (b) JEZ-1 (2 mm), and (c) JEZ-1 (3 mm). Increasing regolith thickness shifts the peak toward lower deposited energies, from ∼68.3 MeV (no regolith) to ∼64.1 MeV (2 mm) and ∼61.8 MeV (3 mm), consistent with increased energy loss in the regolith layer. The peak also broadens with thickness (e.g., σ increases from ∼2.8 MeV to ∼3.7 MeV), reflecting energy straggling and scattering.

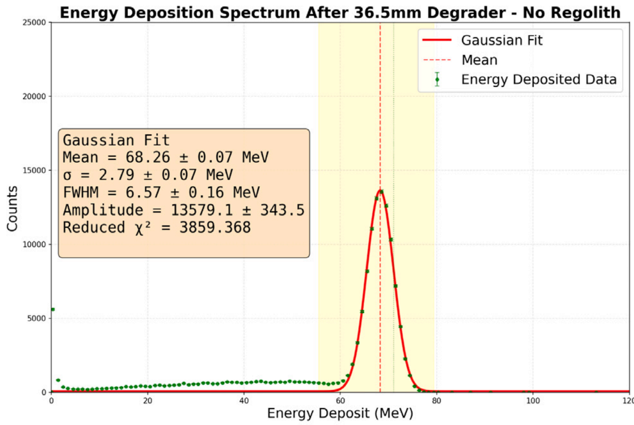

(a) no regolith.

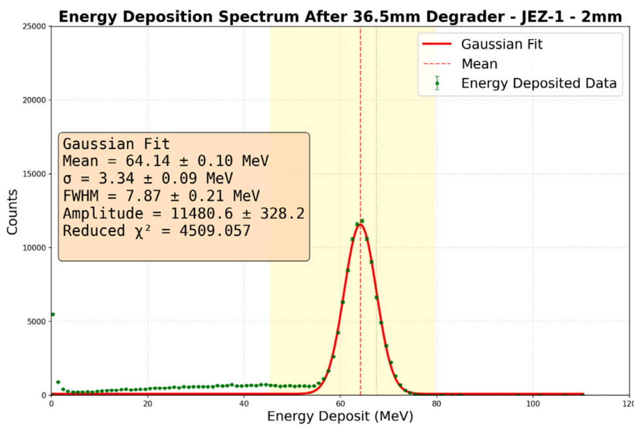

(b) JEZ-1, 2 mm.

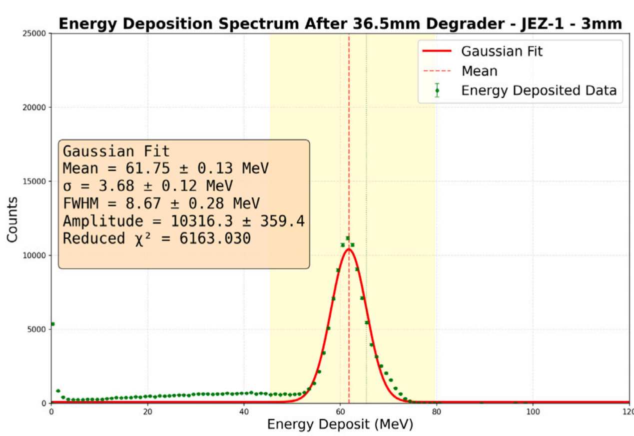

(c) JEZ-1, 3 mm.

Fig. 9. Simulated energy-deposition spectra in the LYSO detector for the 36.5 mm degrader configuration: (a) no regolith, (b) JEZ-1 2 mm, and (c) JEZ-1 3 mm.

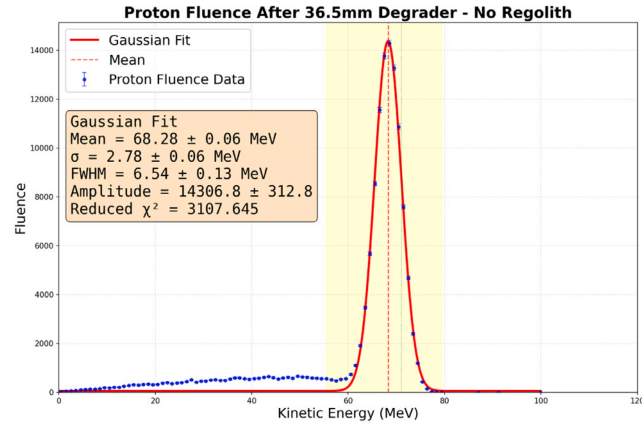

(a) no regolith.

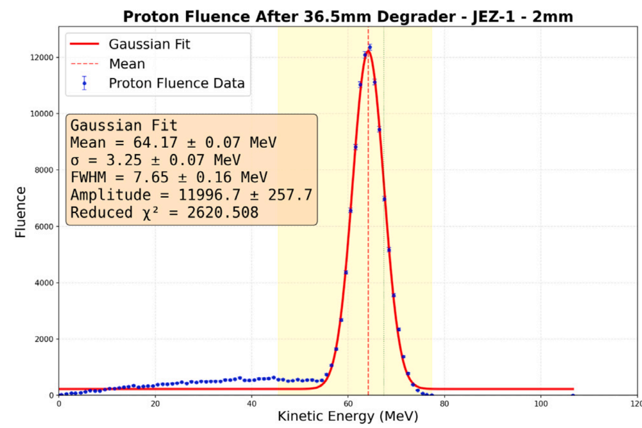

(b) JEZ-1, 2 mm.

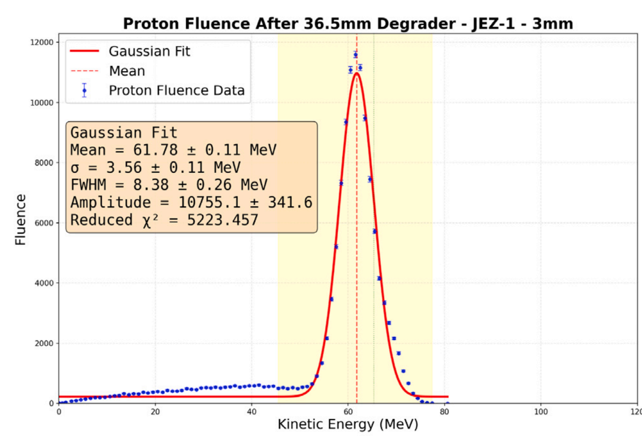

(c) JEZ-1, 3 mm.

Fig. 10. Simulated transmitted-proton fluence spectra for the 36.5 mm degrader configuration: (a) no regolith, (b) JEZ-1 2 mm, and (c) JEZ-1 3 mm.

Fig. 10 presents the transmitted-proton fluence spectra after the 36.5 mm degrader for the same configurations. The fluence peak position, extracted via a Gaussian fit, provides the characteristic transmitted-proton energy reaching the detector region. As the regolith thickness increases, the peak shifts systematically to lower kinetic energies and the distribution becomes broader, indicating thickness-dependent energy degradation and straggling in the regolith. The fitted peak energies decrease from ∼68.3 MeV (no regolith) to ∼64.2 MeV (2 mm) and ∼61.8 MeV (3 mm), in agreement with the corresponding trend observed in the energy-deposition spectra. These representative examples illustrate the peak-extraction workflow that was applied consistently to all simulated configurations.

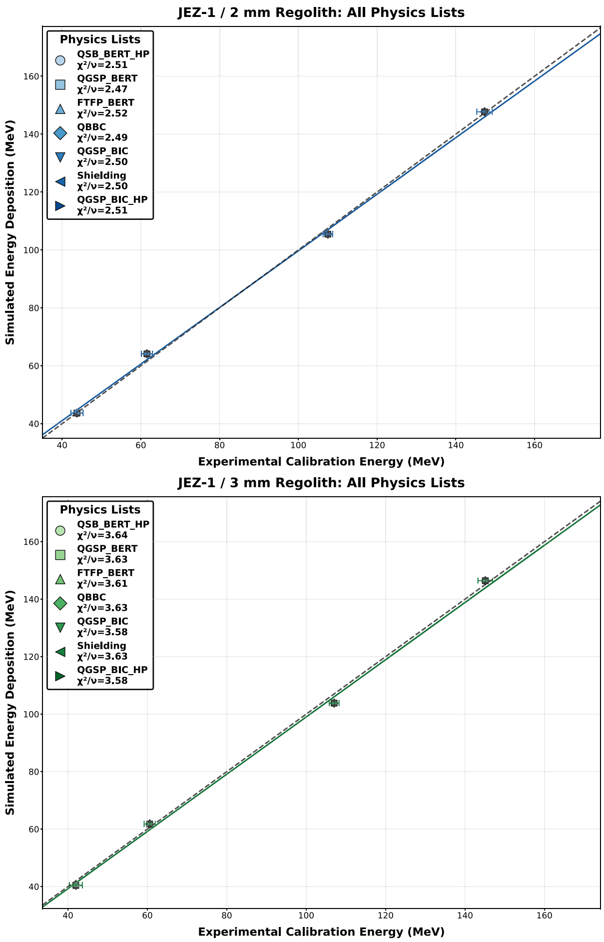

Fig. 11. Simulated versus experimental energies for JEZ-1 at (left) 2 mm and (right) 3 mm thickness for the tested physics lists. A linear fit is applied to the data in each plot to compute the χ^2 and reduced χ^2/ν values for model validation.

3.3. Physics-list benchmarking results

The benchmarking of candidate GEANT4 physics lists against the PIF proton-beam calibration data was performed using an energy-deposition comparison and the reduced-χ^2 criterion to select the model for subsequent Martian simulations.

Table 2 summarizes the results of energy deposition(MeV) inside the LYSO detector for JEZ-1 at 2 mm and 3 mm across all tested physics lists. Fig. 11 compares the simulated energy deposition in the LYSO detector against the corresponding experimentally derived calibration energies for JEZ-1 regolith at thicknesses of 2 mm and 3 mm, for each tested physics list. Fig. 12 summarizes the resulting reduced-χ^2 values for all physics lists, separately for 2 mm (blue) and 3 mm (green). For the 2 mm case, all tested lists yield very similar performance, with reduced-χ^2 values in the narrow range ≈2.47–2.52 (lowest value observed for `QGSP_BERT`, $\chi^2/\nu = 2.47$). For the 3 mm case, the reduced χ^2 values are systematically higher, spanning ≈3.58–3.64, indicating an increased sensitivity of the energy-deposition response to model differences at larger regolith thickness. The lowest χ^2/ν values at 3 mm are obtained for `QGSP_BIC` and `QGSP_BIC_HP` (both $\chi^2/\nu = 3.58$). Although differences between models are small, considering both thicknesses together, `QGSP_BIC` provides the most robust overall agreement and is therefore selected as the best-performing physics configuration for the subsequent Martian-flux simulations.

3.4. Experimental–simulation comparison

In this section, experimental results are quantitatively compared with simulations to assess the agreement in proton energy and fluence. Fig. 13 presents the normalized energy difference as a function of experimental proton energy for the regolith-free configuration. Fig. 14 compares the thickness dependence of proton energy obtained from experimental data and simulations. Both datasets exhibit a consistent linear decrease of energy with increasing degrader thickness, with comparable slopes and correlation coefficients, demonstrating that the simulation reproduces the experimentally observed energy degradation trend.

Table 3 summarizes the experimental calibration outputs and the corresponding simulation results for all degrader and regolith configurations. The “Degrader” column denotes the thickness (in mm) of the upstream energy-degrading absorber used in the PIF setup to reduce the nominal 200 MeV beam to the desired proton energy at the regolith surface. For each configuration, the experimental detector-response peak (“Mean of mV [fit]”) was converted to a calibrated peak energy (“Calib. Energy”) using the no-regolith calibration, and compared to the simulated energy deposition in the LYSO detector. The last column reports the relative difference between simulation and experiment, showing generally good agreement across configurations (typically within a few percent, with the largest deviation occurring at the lowest-energy no-regolith point). Here, “Energy Deposition” and “Proton Fluence” denote the Gaussian-peak observables extracted from the simulated spectra in the LYSO volume using identical scoring definitions across runs. In the energy deposition dataset below, values reported as *Mean* ± correspond to the Gaussian peak position μ and its 1σ statistical uncertainty (standard error) obtained from the fit covariance matrix.

4. Conclusions

This technical report documents the comparison and validation of proton-beam measurements performed at the Proton Irradiation Facility (PIF) with MRADSIM simulations for Martian regolith. Spark Plasma Sintering (SPS) was used at the University of Cagliari to produce the materials to be tested with future aim of evaluating their radiation shielding on Mars. To this two different types of regolith simulant (JEZ-1 and MGS-1) were processed by SPS to provide 2 and 3 mm thick disks, which were irradiated with proton energies spanning approximately 29.3–150 MeV at the regolith surface. These energies were obtained by using copper degraders of varying thicknesses downstream of an initial proton beam energy of 200 MeV.

The PIF experimental setup includes beamline instrumentation comprising a series of degraders for energy adjustment, a collimator, several ionization chambers for beam monitoring, and a downstream detector system used to measure the particle response. SE2S team provided the experimental spectra in four-column datasets: the first column corresponds to the bin index, the second and third columns define the lower and upper edges of the detector signal-amplitude bins (in mV), and the fourth column gives the number of counts recorded in each bin. Using the regolith-free calibration data supplied by PIF—specifically, signal amplitude (mV) versus energy—a conversion function was derived to determine particle energies from measured signal amplitudes for all subsequent experimental configurations, including those involving different degrader settings and regolith samples. Peak energies were extracted consistently via Gaussian fits to the dominant spectral features.

The complete PIF beamline geometry, provided in GDML format, was implemented in the MRADSIM simulation framework, and all experimental configurations were simulated accordingly. Candidate GEANT4 physics lists were benchmarked against the PIF proton-beam calibration energies for JEZ-1 at 2 mm and 3 mm using an energy-deposition comparison and a reduced-χ^2/ν criterion, leading to the

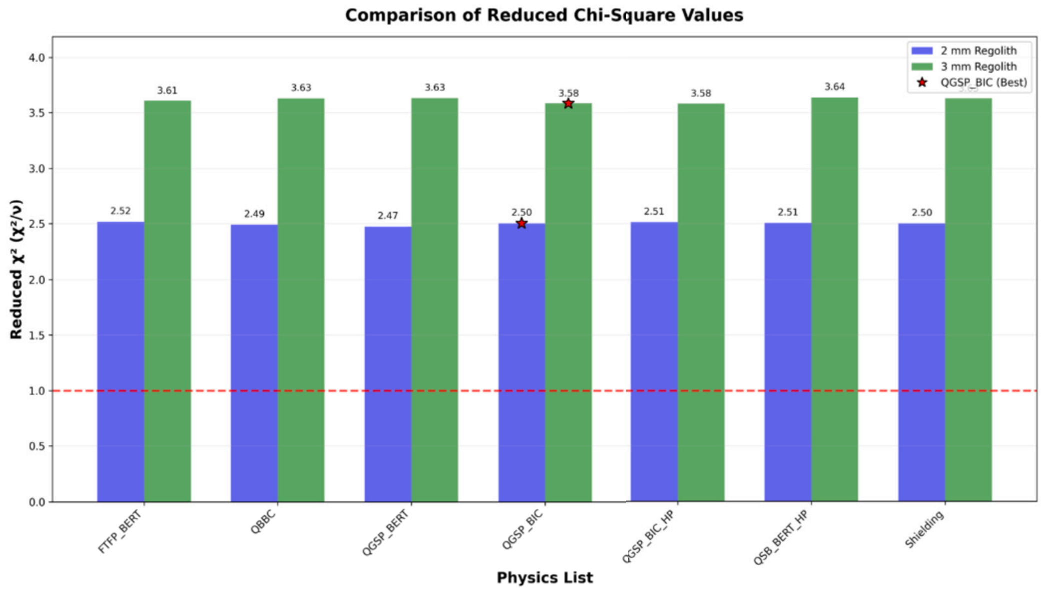

Fig. 12. The reduced chi-square (χ^2/ν) was computed for each physics list for the JEZ-1 regolith configuration. The blue bars represent the results for the 2 mm thickness, while the green bars correspond to the 3 mm thickness. The physics list exhibiting the lowest average reduced chi-square across both thicknesses — `QGSP_BIC` in this case — is identified as the best-performing model.

Table 2
PIF degrader benchmark for JEZ-1 regolith (2 mm and 3 mm): calibration energies and MRADSIM-simulated energy deposition (MeV) for the tested physics lists (mean ± uncertainty).

Degrader (mm)	Regolith thickness	Calibration energy (MeV)	Energy deposition (MeV)							Percentage difference (%)
			QGSP_BERT_HP	QGSP_BERT	FTFP_BERT	QBBC	QGSP_BIC	Shielding	QGSP_BIC_HP	
16.5	JEZ-1/2 mm	147.3 ± 2.0	147.7 ± 0.05	147.7 ± 0.05	147.7 ± 0.05	147.7 ± 0.07	147.7 ± 0.07	147.7 ± 0.07	147.7 ± 0.07	+0.3
28	JEZ-1/2 mm	107.5 ± 1.2	105.5 ± 0.05	105.5 ± 0.05	105.4 ± 0.05	105.5 ± 0.05	105.5 ± 0.05	105.5 ± 0.05	105.5 ± 0.05	−1.9
36.5	JEZ-1/2 mm	61.6 ± 1.4	64.2 ± 0.08	64.1 ± 0.08	64.1 ± 0.08	64.1 ± 0.09	64.1 ± 0.08	64.1 ± 0.09	64.1 ± 0.08	+4.2
39.5	JEZ-1/2 mm	43.8 ± 1.6	43.7 ± 0.03	43.7 ± 0.11	43.6 ± 0.06	43.7 ± 0.14	43.7 ± 0.05	43.7 ± 0.06	43.7 ± 0.06	−0.3
16.5	JEZ-1/3 mm	145.1 ± 1.9	146.4 ± 0.05	146.4 ± 0.05	146.4 ± 0.06	146.4 ± 0.06	146.4 ± 0.07	146.4 ± 0.07	146.4 ± 0.04	+0.9
28	JEZ-1/3 mm	107.0 ± 1.2	103.8 ± 0.05	103.8 ± 0.05	103.8 ± 0.05	103.8 ± 0.04	103.8 ± 0.05	103.8 ± 0.05	103.8 ± 0.05	−3.0
36.5	JEZ-1/3 mm	60.6 ± 1.4	61.8 ± 0.12	61.8 ± 0.12	61.8 ± 0.12	61.8 ± 0.13	61.8 ± 0.11	61.8 ± 0.13	61.8 ± 0.13	+2.0
39.5	JEZ-1/3 mm	42.0 ± 1.6	40.4 ± 0.13	40.4 ± 0.11	40.5 ± 0.13	40.4 ± 0.12	40.5 ± 0.05	40.4 ± 0.13	40.5 ± 0.14	−3.6

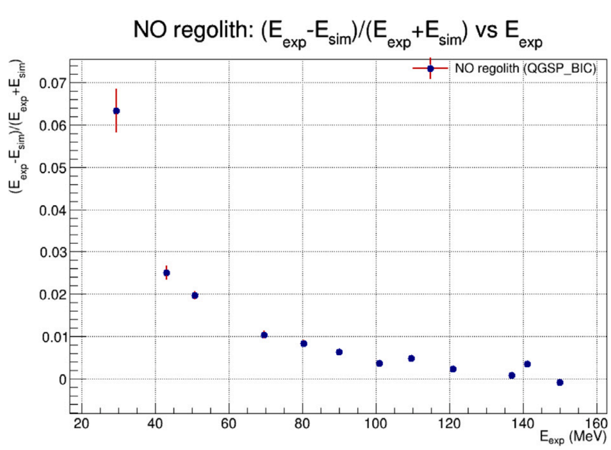

Fig. 13. Normalized energy difference as a function of experimental proton energy for the no-regolith configuration. For the no-regolith configuration, the normalized energy difference remains centered around zero across the full energy range, indicating very good agreement between experiment and simulation, with larger uncertainties at lower energies due to increased straggling and statistical fluctuations.

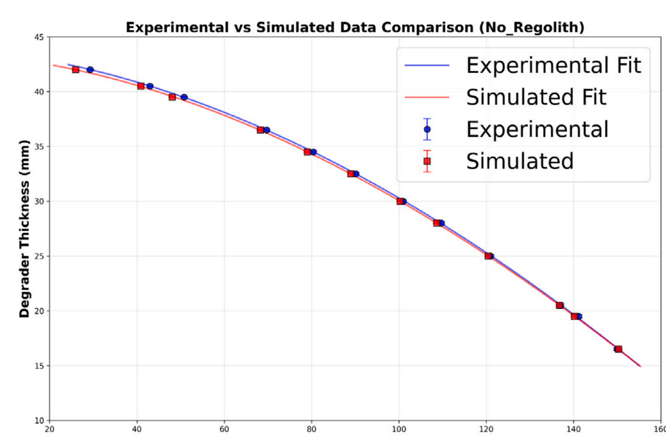

Fig. 14. Proton energy as a function of degrader thickness obtained from experimental data and simulations. Quadratic fits are shown for both datasets to illustrate the thickness-dependent energy degradation.

Table 3
Experimental calibration results and corresponding simulation outputs for all degrader/regolith configurations. Uncertainties are given as $\pm 1\sigma$.

Degrader (mm)	Regolith	Thickness (mm)	E_0 (MeV)	Experimental		Simulation		
				Mean of mV [fit]	Calib. energy (MeV)	Energy deposition (MeV)	Proton fluence	Percentage difference (%)
16.5	NO	0	200	0.359828	150 ± 0.11	150.25 ± 0.03	81 444 ± 1651.3	0.17
19.5	NO	0	200	0.341268	141.2 ± 0.15	140.22 ± 0.07	54 064.4 ± 2936.1	−0.69
20.5	NO	0	200	0.322465	137 ± 0.15	136.78 ± 0.05	50 056.2 ± 2186.5	−0.16
25.0	NO	0	200	0.309474	121 ± 0.10	120.45 ± 0.03	32 065.7 ± 511.1	−0.45
28.0	NO	0	200	0.285641	109.7 ± 0.12	108.66 ± 0.05	22 995.7 ± 509.1	−0.95
30.0	NO	0	200	0.266116	101 ± 0.11	100.26 ± 0.02	17 457.2 ± 176.7	−0.73
32.5	NO	0	200	0.235434	90.1 ± 0.11	88.98 ± 0.03	26 272.1 ± 900	−1.24
34.5	NO	0	200	0.208012	80.4 ± 0.11	79.06 ± 0.07	19 129.3 ± 582.9	−1.67
36.5	NO	0	200	0.175010	69.7 ± 0.09	68.27 ± 0.09	14 272.8 ± 369.3	−2.05
39.5	NO	0	200	0.121493	50.8 ± 0.06	48.83 ± 0.08	7707.9 ± 187.3	−3.88
40.5	NO	0	200	0.099329	43.0 ± 0.07	40.90 ± 0.12	6370.4 ± 220.5	−4.88
42.0	NO	0	200	0.060864	29.3 ± 0.08	26.43 ± 0.26	3441.4 ± 188.6	−9.80
16.5	MGS-1	2	200	0.353900	147.01 ± 1.94	147.80 ± 0.03	79 265.1 ± 1566.9	0.54
28.0	MGS-1	2	200	0.279100	107.83 ± 1.20	105.56 ± 0.05	22 215 ± 423.6	−2.11
36.5	MGS-1	2	200	0.164400	63.07 ± 1.42	64.28 ± 0.09	12 146 ± 235	1.92
39.5	MGS-1	2	200	0.108100	44.65 ± 1.52	43.66 ± 0.19	5943.4 ± 272	−2.22
16.5	MGS-1	3	200	0.350100	144.99 ± 1.84	146.55 ± 0.03	77 723.5 ± 1327.2	1.08
28.0	MGS-1	3	200	0.272100	106.62 ± 1.23	103.99 ± 0.05	21 792.2 ± 414	−2.47
36.5	MGS-1	3	200	0.154100	59.47 ± 1.39	62.02 ± 0.13	10 807.4 ± 332.5	4.29
39.5	MGS-1	3	200	0.095800	41.02 ± 1.68	40.86 ± 0.16	4917.5 ± 160.9	−0.39
16.5	JEZ-1	2	200	0.354400	147.28 ± 1.96	147.72 ± 0.03	79 403.1 ± 1503.3	0.30
28.0	JEZ-1	2	200	0.274000	107.49 ± 1.22	105.47 ± 0.05	22 327 ± 407.3	−1.88
36.5	JEZ-1	2	200	0.160100	61.55 ± 1.40	64.15 ± 0.10	11 977.6 ± 240.4	4.22
39.5	JEZ-1	2	200	0.105200	43.78 ± 1.55	43.59 ± 0.11	5937.6 ± 146.4	−0.43
16.5	JEZ-1	3	200	0.350300	145.10 ± 1.85	146.44 ± 0.03	77 631 ± 1314.8	0.92
28.0	JEZ-1	3	200	0.273000	107.03 ± 1.23	103.84 ± 0.05	21 803.1 ± 418.1	−2.98
36.5	JEZ-1	3	200	0.157300	60.58 ± 1.40	61.76 ± 0.13	10 793.1 ± 344	1.95
39.5	JEZ-1	3	200	0.099100	41.98 ± 1.63	40.56 ± 0.17	4852.1 ± 160.6	−3.38

selection of QGSP_BIC as the most robust baseline for subsequent Martian-flux simulations. Using the selected physics list, the simulated LYSO peak energy deposition reproduces the calibrated experimental peak energies with good overall agreement: the relative differences are typically within a few percent across most degrader and regolith configurations, and remain below 10% for the full dataset. The largest deviation is observed for the lowest-energy, no-regolith configuration (calibrated peak energy ∼29.3 MeV), where the simulation underestimates the experimental value by ∼9.8%.

Detailed information on systematic uncertainties in the experimental setup—such as detector energy resolution, counting efficiency, uncertainties in measured distances, and degrader thickness tolerances—was not available. Nevertheless, considering the statistical uncertainties from the Gaussian fits and the observed residuals across configurations, the combined experimental uncertainty is expected to be at the few-percent level, potentially approaching the ∼5–10% range for the lowest-energy cases.

CRediT authorship contribution statement

Zehra Guzel: Writing – original draft, Visualization, Validation, Software, Investigation, Formal analysis, Data curation. **Muhammad Waqas:** Writing – original draft, Validation, Supervision, Software, Data curation. **Ali Behcet Alpat:** Writing – review & editing, Validation, Supervision, Funding acquisition. **Talifujiang Wusimanjiang:** Visualization, Software, Resources, Methodology. **Celal Mert Okan:** Visualization, Software. **Deniz Dolek:** Software. **Efe Alpat:** Resources, Project administration. **Mariano Casu:** Supervision, Project administration, Investigation, Conceptualization. **Roberto Orrù:** Validation, Supervision, Data curation, Conceptualization. **Giacomo Cao:** Supervision, Investigation, Funding acquisition, Conceptualization. **Wojtek Hajdas:** Software, Formal analysis, Data curation. **Radoslaw Marcinkowski:** Software, Formal analysis, Data curation.

Declaration of competing interest

The authors declare that they have no known competing financial interests or personal relationships that could have appeared to influence the work reported in this paper.

Acknowledgments

The authors thank the SE2S team for providing the proton-beam dataset and geometry files. Mariano Casu performed his activity in the framework of the Ph.D. in Innovation Sciences and Technologies at the University of Cagliari, Italy. The contribution of Prof. Roberta Licheri and Prof. Alessandro Concas from the University of Cagliari is gratefully acknowledged. This work has been developed within the framework of the project "SMS—Space Manufacturing in-situ—Realizzazione in contesti spaziali di manufatti" project (cod. ARS01_01361), sponsored by the Italian Ministry of University and Research, (MUR), Italy (Cod. CUP: B25F21001330005).

Data availability

Data will be made available on request.

References

[1] S. Khaksari, D. Matthiae, et al., Radiation transport through the martian atmosphere as a function of the Zenith angle, J. Geophys. Res.: Planets (2025) http://dx.doi.org/10.1029/2025JE009352.

[2] M.Z. Naser, Extraterrestrial construction materials, Prog. Mater. Sci. 105 (2019) 100577, http://dx.doi.org/10.1016/j.pmatsci.2019.100577.

[3] J. Albrecht, et al., Global tuning of hadronic interaction models with accelerator-based and astroparticle data, Nat. Rev. Phys. 8 (2026) 98–114, http://dx.doi.org/10.1038/s42254-025-00897-3, Published online 16 Dec 2025.

[4] D. Karl, K.M. Cannon, A. Gurlo, Review of space resources processing for Mars missions: Martian simulants, regolith bonding concepts and additive manufacturing, Open Ceram. 9 (2022) 100216, http://dx.doi.org/10.1016/j.oceram.2021.100216.

[5] H. Llamas, K. Aplin, L. Berthoud, Effectiveness of Martian regolith as a radiation shield, Planet. Space Sci. 218 (2022) http://dx.doi.org/10.1016/j.pss.2022.105517.

[6] J.M. DeWitt, E.R. Benton, Secondary proton buildup in space radiation shielding, Life Sci. Space Res. 41 (2024) 119–126, http://dx.doi.org/10.1016/j.lssr.2024.02.005.

[7] N. Costa, A. Bonetto, P. Ferretti, et al., Analytical data on three Martian simulants, Data Brief (2024) 111099, http://dx.doi.org/10.1016/j.dib.2024.111099.

[8] W. Hajdas, L. Adams, B. Nickson, A. Zehnder, The proton irradiation facility at the paul scherrer institute, Nucl. Instrum. Methods Phys. Res. B 113 (1) (1996) 54–58, http://dx.doi.org/10.1016/0168-583X(95)01327-X.

[9] M. Casu, R. Licheri, D. Bambas, F. Aymerich, L. Cappai, A. Concas, G. Cao, R. Orrù, Enhanced properties by spark plasma sintering of additive-free Martian soil simulants for ISRU applications, Ceram. Int. 51 (24) (2025) 42046–42058, http://dx.doi.org/10.1016/j.ceramint.2025.06.423.

[10] A.B. Alpat, et al., MRADSIM (Matter-RADiation Interactions SIMulations), 2024, http://dx.doi.org/10.48550/arXiv.2411.11173, arXiv:2411.11173.

[11] S. Agostinelli, et al., GEANT4 - a simulation toolkit, Nucl. Instrum. Methods Phys. Res. A 506 (3) (2003) 250–303, http://dx.doi.org/10.1016/S0168-9002(03)01368-8.

[12] A.B. Alpat, A. Coban, H. Kaya, G. Bartolini, MRADSIM-converter: A new software for STEP to GDML conversion, Comput. Phys. Comm. 286 (2023) 108688, http://dx.doi.org/10.1016/j.cpc.2023.108688.

[13] N. Ciccarella, S.G. Avsar, A.B. Alpat, G. Bartolini, T. Wusimanjiang, L. Salvi, S. Gigli, H. Raheem, A.I. Shah, U. Gokmen, S.B. Ocak, New radiation shielding material studies for space-borne and earth-based application using MRADSIM software toolkit, J. Instrum. 20 (06) (2025) T06002, http://dx.doi.org/10.1088/1748-0221/20/06/T06002.

[14] Exolith-Lab, MGS-1 Mars Global Simulant fact sheet, 2018, https://sciences.ucf.edu/class/wp-content/uploads/sites/23/2018/11/Spec_MGS-1.pdf. (Accessed 13 March 2026).

[15] Exolith-Lab, JEZ-1 Jezero Delta simulant fact sheet, 2019, https://www.sciences.ucf.edu/class/wp-content/uploads/sites/23/2019/02/Spec_JEZ-1.pdf. (Accessed 13 March 2026).

[16] Geant4 Collaboration, Guide for physics lists, 2024, https://geant4-userdoc.web.cern.ch/UsersGuides/PhysicsListGuide/html/index.html. (Accessed 12 May 2025).

[17] Geant4 Collaboration, Geant4 11.3 release notes, 2024, https://geant4.orgdownload/release-notes/notes-v11.3.0.html. (Accessed 05 March 2026).

[18] F. Horst, et al., A multi-detector experimental setup for the study of space radiation shielding materials: measurement of secondary radiation behind thick shielding, EPJ Web Conf. 261 (2022) 03002, http://dx.doi.org/10.1051/epjconf/202226103002.

[19] D.H. Wright, M.H. Kelsey, The Geant4 Bertini cascade, Nucl. Instrum. Methods Phys. Res. A 804 (2015) 175–188, http://dx.doi.org/10.1016/j.nima.2015.09.058.